OBSERVING THE MARTIAN ATMOSPHERE USING ENTRY PROBE FLIGHT INSTRUMENTATION

B. Van Hove, **Ö. Karatekin**, *Royal Observatory of Belgium, Ukkel, Belgium*

Introduction:

In 1971, Mariner 9 became the first probe to orbit Mars. After the subsequent Viking landers and a period of reduced interest in Mars, the years 1995 to 2005 saw a surge of dedicated Mars missions. Many of these were orbiting platforms: Mars Global Surveyor (MGS)[1], Mars Odyssey[2], Mars Express[3] and Mars Reconnaissance Orbiter (MRO)[4]. Apart from MGS, all are still operational today and have accumulated a wealth of Martian atmosphere observations[5]. Landed platforms have probed the atmosphere from the Martian surface, e.g. Mars Pathfinder[6], Mars Phoenix[7] and recently Curiosity[8].

During their atmospheric entry, landers record acceleration and rotation rate histories using Inertial Measurement Units (IMU). These have been used in conjunction with atmospheric drag estimates to reconstruct spatially and temporally narrow but high resolution thermodynamic profiles of density, pressure and temperature along the entry trajectory[9,10,11]. The profiles exhibit large-scale oscillations consistent with thermal tides[12], correlations with dust opacity have also been suggested[13]. Pathfinder's observations from the surface as well as its flight reconstruction have indicated the presence of CO_2 clouds on Mars [14,15].

In this growing collection of Mars atmosphere data, there are no direct observations of middle to high altitude winds, neither from orbiters nor in-situ. Since landers traverse the full vertical range of the atmosphere, they are candidates for in-situ wind measurements. During most of the entry however, they travel at speeds far in excess of the local wind velocity, so the accelerations recorded by IMU convey practically no information on local winds.

Mars Science Laboratory (MSL) recently became the first lander to fly an instrumented heat shield through the Martian atmosphere[16]. Its grid of pressure sensors is called a Flush Air Data System (FADS)[17]. The addition of heat shield surface pressure measurements allows for atmosphere reconstruction without reliance on aerodynamic drag estimates. Potentially, FADS can even resolve wind velocity. FADS is also installed on ESA's 2016 ExoMars EDL Demonstrator Module (EDM)[18].

We quantify the accuracy of atmospheric profile reconstruction from simulated EDM flight data with and without complementary FADS instrumentation, and demonstrate that resolving atmospheric winds can be of importance for post-flight reconstruction. While the FADS instrumentation on EDM is likely not sufficient to accurately resolve winds, we provide preliminary requirements for FADS sensors that are.

Atmospheric entry flight simulator:

We developed a simulator that generates flight trajectories with associated flight measurement data. In a simulation, all relevant parameters such as local atmospheric conditions, aerodynamics and flight instrumentation are configurable and known.

The simulator solves a system of six degree of freedom (6-DOF) equations of motion from an initial state. Mars is represented by an oblate ellipsoid, two degree harmonic gravity model, planet rotation rate and atmospheric profiles. Gravitational and aerodynamic forces carry the lander along its trajectory.

To validate the flight simulator, we conducted a case study of the Phoenix entry. High quality, publically available IMU data and a reproducible flight anomaly make Phoenix a useful validation case. On May 2008, Phoenix successfully landed on Mars. It was equipped with the most accurate IMU yet[19]. Post-flight trajectory reconstruction revealed a discrepancy between the flown and expected attitude, which had not been present in pre-flight simulations. Two potential sources for the attitude anomaly were proposed: a center of gravity (CG) offset or a static stability (C_m) misprediction, both relatively small. The observed attitude history was successfully approximated by tuning these two parameters in ad-hoc simulations[20].

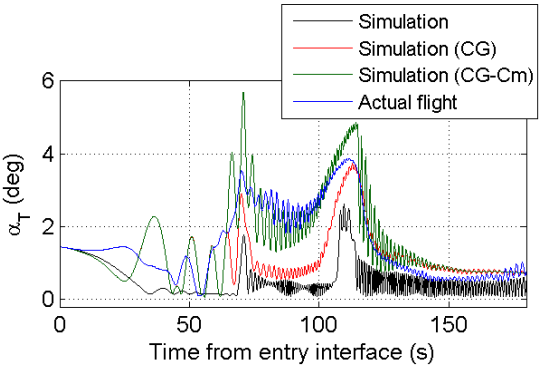

Fig. 1. Phoenix simulated vs. flown attitude history

Fig. 1 shows four Phoenix attitude histories where α_T is total angle of attack. The blue line is the post-flight reconstruction, the black line our own 'pre-flight' trajectory simulation. As in independent simulations[20], two known aerodynamic instabilities are resolved but not the observed attitude anomaly.

We proceed to first add only a radial CG offset

and second also a static C_m deviation, using the same offset values as [20]. This approximately resolves the attitude discrepancy and demonstrates the correct implementation of the flight simulator.

Atmospheric profile reconstruction methods:

From IMU data. Reconstructing the flight trajectory is a necessary first step before deriving atmospheric profiles. Acceleration and rotation rate histories from the IMU can be numerically integrated over time to derive the flight trajectory in an inertial frame. The density profile is then derived from the drag equation which relates acceleration, air speed, aerodynamic drag coefficient and density. Hydrostatic equilibrium and the ideal gas law are then employed to derive pressure and temperature[21].

From IMU+FADS data. The IMU method relies on an assumed aerodynamic drag coefficient[22] and on air speed. Since IMU data provides velocity w.r.t. an inertial planet centered frame, planet rotation and wind velocity must be assumed to estimate air speed. The interest of FADS data processing for atmosphere reconstruction lies in its independence of knowledge of aerodynamic drag and the possibility to derive wind velocity to improve air speed estimation.

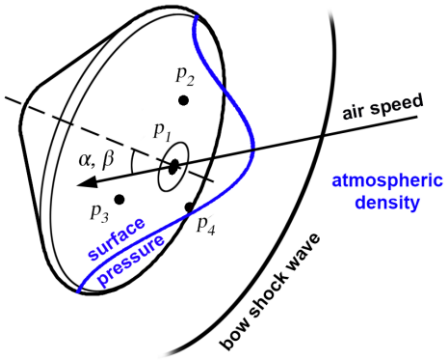

Fig. 2. FADS atmosphere reconstruction

Fig. 2 illustrates how atmospheric density can be reconstructed from heat shield surface pressure measurements p_i. This involves estimation of the air speed vector, its direction decomposed in flow incidence angles α and β. The derivation of upstream flow conditions such as density requires modeling the shock wave. Our FADS solver[21] assumes a modified Newtonian flow surface pressure distribution, and solves normal shock wave conservation equations using CO_2 properties from a high temperature thermodynamic library developed at the von Karman Institute[23].

Because wind velocity affects the heat shield surface pressure distribution, it can be derived from it. However, because the wind velocity is low compared to the air speed, the surface pressure distribution is only slightly affected and very sensitive FADS sensors are required to detect winds. This becomes apparent in the following ExoMars EDM case study.

ExoMars EDM atmosphere reconstruction:

EDM is the first of two ESA-Roscosmos Mars missions scheduled for 2016 and 2018. If successful, EDM will be Europe's first landing on Mars. It will enter the Martian atmosphere at an altitude of 120 km with a velocity of 6 km/s from a location near the Equator. Solar longitude will be about 244°[24] which is in the Martian dust season characterized by highly variable weather and increased likelihood of global dust storms. ExoMars EDM and the similarly timed NASA InSight[25] are the first opportunities to observe Martian dust storms during entry.

Flight data simulation. Both IMU and FADS data were simulated from interface at 120 km to an altitude of about 6 km above ground level, approximately at parachute deployment. Detailed aerodynamics similar to those of Phoenix were used.

Atmosphere profiles were extracted from the Mars Climate Database (MCD). These are density, pressure, temperature, molecular weight, heat capacity ratio, dynamic viscosity and three-component winds, all varying with altitude. MCD is an inventory of LMD Mars Global Circulation Model (GCM)[26] solutions for multiple weather scenarios. We considered normal and global dust storm scenarios, the latter based on high dust opacity estimates from [27].

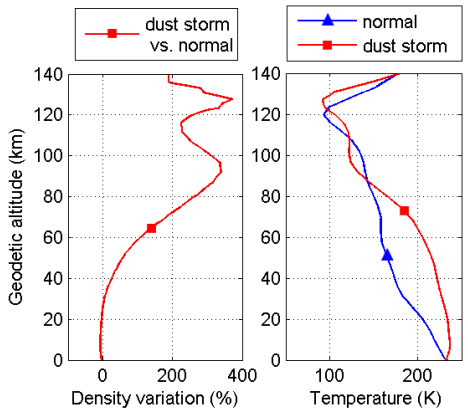

Fig. 3. MCD normal and dust storm profiles

Fig. 3 compares density and temperature profiles between both weather scenarios. Density variations are relatively large but do not affect the trajectory much due to low absolute density at high altitudes. The largest temperature variations between the two scenarios occur between 20 and 80 km. Fig. 4 compares wind profiles. Very fast retrograde winds are predicted, exceeding 200 m/s above 80 km in the dust scenario. These are caused by migrating thermal tides due to solar heating forcing, which drag the atmosphere toward the sub-solar point[28]. Predicted wind speeds in the normal weather scenario are smaller by about a factor two.

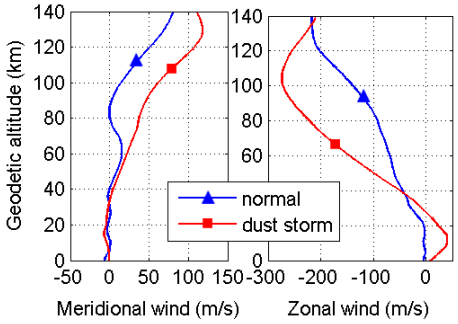

Fig. 4. MCD normal and dust storm wind profiles

The simulated flight data is very similar for both scenarios; we show only that for the global dust storm scenario. Fig. 5 shows acceleration histories, of which the axial component is by far the largest. Fig. 6 shows FADS pressure signals, largest at peak deceleration. All signals start out close to zero, where pressure and density are negligible.

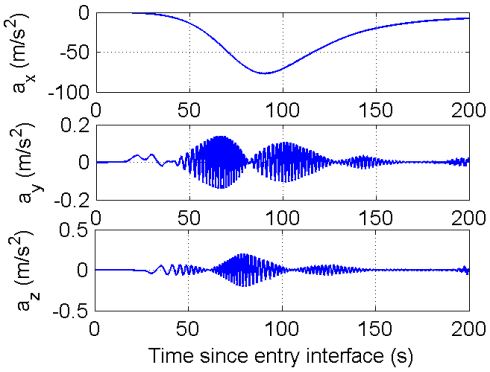

Fig. 5. Simulated EDM accelerometer signals

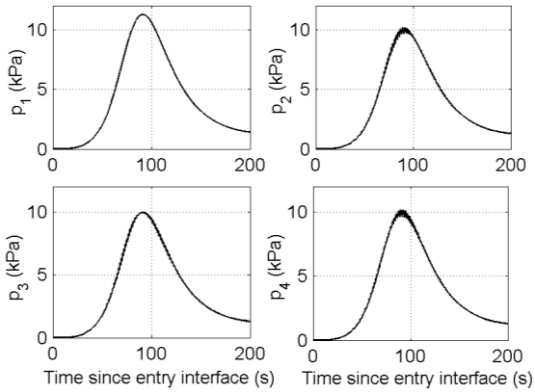

Fig. 6. Simulated EDM FADS surface pressure signals

Atmosphere reconstruction. The simulated flight data was provided to the reconstruction methods described above in a Monte Carlo analysis. Gaussian distributed uncertainties were imposed on all input parameters, excluding the modified Newtonian pressure distribution model which is considered a placeholder for higher fidelity models[29]. For the FADS sensors on EDM we considered 3-σ noise errors of ± 35 Pa and 3-σ sensor position errors of ± 1 mm.

Fig. 7 shows the total 3-σ uncertainty (top) including bias error, and the bias error separately (bottom) for the reconstructed density profile in the global dust storm scenario. The profile was reconstructed using either only IMU data (drag method), or using IMU+FADS data. When including FADS, the air speed estimator can either assume zero winds or attempt to correct air speed with a wind estimate:

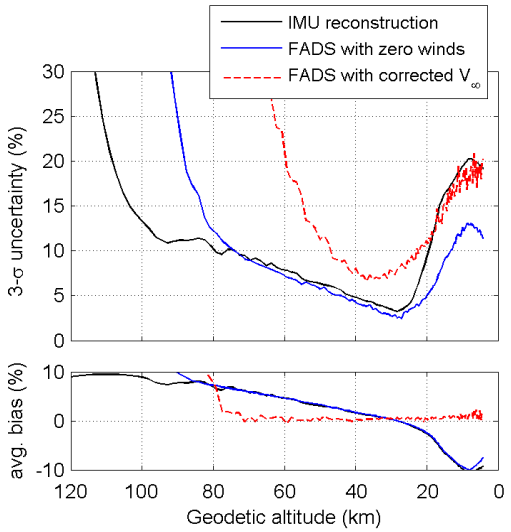

Fig. 7. Monte Carlo results for density profile reconstruction (global dust storm scenario)

Above 80 km, poor signal-to-noise prevents accurate reconstruction. Below 30 km, increasing drag coefficient uncertainty affects IMU only reconstruction, while decreasing signal-to-noise affects the FADS reconstructions. Nevertheless, FADS (zero winds) compares favorably to IMU reconstruction below 30 km. The methods that assume zero winds suffer from significant bias error due to poor air speed estimations. Attempting to correct air speed with FADS wind estimates is actually detrimental: on average the bias error is removed but replaced by high variance of the wind estimate. For the preliminary EDM FADS sensor uncertainties, atmospheric winds are thus poorly constrained.

Fig. 8 compares density and temperature reconstruction uncertainty for between weather scenarios. Reduced winds for normal weather result in a smaller but still significant bias error. Temperature reconstruction is less sensitive to neglecting winds as correlated bias errors on density and pressure are partially cancelled out in the ideal gas law.

Wind estimation. FADS data simulated for EDM was not able to constrain winds. Wind estimation can be improved by installing more and/or more accurate pressure sensors. We now consider eight sensors (MSL carried seven) and estimate percentage noise error required to estimate winds sufficiently accurately to improve atmospheric profile reconstruction through a better air speed estimate. Note that a perfect surface pressure model is assumed: future investigations will include complete model uncertainty.

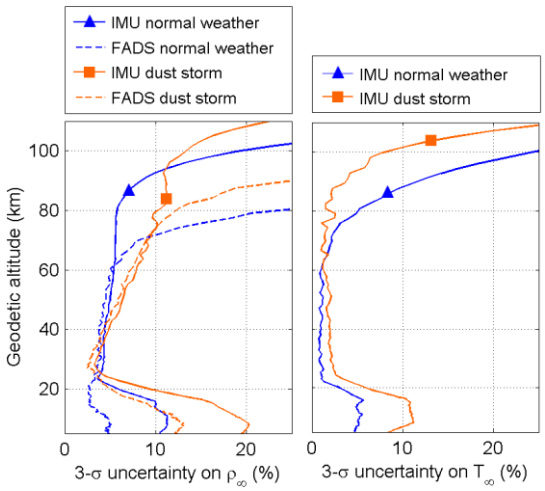

Fig. 8. Reconstruction uncertainty for both scenarios

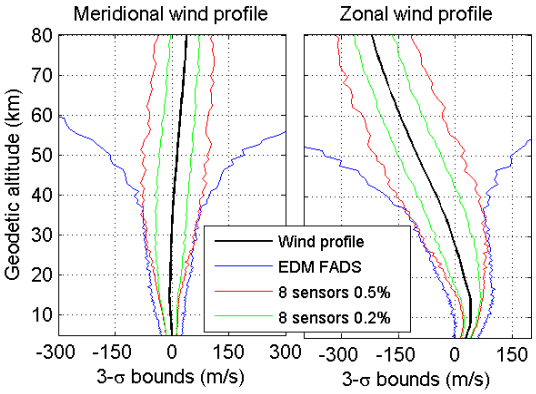

Fig. 9. Wind reconstruction uncertainty for multiple FADS configurations (global dust storm scenario)

Fig. 9 shows wind estimation performance assuming ± 0.5% and ±0.2% sensor noise (3-σ) over the entire altitude range. With ± 0.5% noise, estimation uncertainty is similar to the best performance of the EDM sensors, i.e. insufficient to improve on the zero wind reconstructions as shown in Fig. 7. Reducing sensor noise to ± 0.2% improves wind estimation considerably. 3-σ uncertainty on the reconstructed winds varies from ±15-10 m/s at 6 km to ± 40-50 m/s at 30 km, above which it remains approximately constant. Incorporating these wind estimates in the air speed improves atmosphere reconstruction: density profile uncertainty is reduced to ± 3% above 40 km, below which it increases to ± 10% at 6 km.

Conclusions:

Heat shield instrumentation (FADS) is a valuable addition to conventional IMU sensors for post-flight atmospheric profile reconstruction. According to the present uncertainty analysis for ExoMars EDM 2016, FADS can improve atmospheric density reconstruction uncertainty below 30 km while assuming zero winds. Neglecting strong retrograde winds predicted by the GCM results in significant atmospheric profile reconstruction error. The four FADS sensors on EDM will likely not be able to constrain those winds. We showed that eight sensors allow for estimation of wind profiles in a given altitude range, if they are accurate to ± 0.2% (3-σ) in that range. Future work will refine these estimates.

References:

[1] A. L. Albee et al., Overview of the Mars Global Surveyor mission, J. Geophys. Res., Vol. 106 Issue E10, pp. 23291-316, (2001). **[2]** Jet Propulsion Laboratory (JPL), NASA Facts: 2001 Mars Odyssey, `http://www.jpl.nasa.gov/news/fact_sheets/Odyssey0302.pdf` on 12 Nov 2013. **[3]** European Space Agency (ESA), Mars Express: The Scientific Payload, ESA SP-1240, (2004). **[4]** R. W. Zurek & S. E. Smrekar, An overview of the Mars Reconnaissance Orbiter (MRO) science mission, J. Geophys. Res., Vol. 112 Issue E5, (2007). **[5]** M. D. Smith, Spacecraft Observations of the Martian Atmosphere, Annu. Rev. Earth Planet. Sci., Vol. 36, pp. 191-219, (2008). **[6]** Anderson et al., Overview of the Mars Pathfinder Mission, Launch through Landing, Surface Operations, Data Sets, and Science Results, J. Geophys. Res., (1998). **[7]** P. H. Smith et al., Overview of the Phoenix Mars Lander Mission, 4th Mars Polar Science Conference, (2006). **[8]** Science 341, five Research Article Special about Curiosity at Gale Crater, (2013). **[9]** J. A. Magalhães et al., Results of the Mars Pathfinder atmospheric structure investigation. J. Geophys. Res., Vol. 104, pp. 8943–56, (1999). **[10]** P. Withers & M. D. Smith, Atmospheric entry profiles from the M Spirit and Opportunity, Icarus, Vol. 185, pp. 133-142, (2006). **[11]** A. Seiff, Atmospheres of Earth, Mars, and Venus, as Defined by Entry Probe Experiments, J. Spacecraft, Vol. 28, No. 3, pp. 265-275, (1991). **[12]** P. Withers & D. C. Catling, Observations of atmospheric tides on Mars at the season and latitude of the Phoenix atmospheric entry, Geophys. Res. Letters, Vol. 37, L24204, (2010). **[13]** M. R. Chizek et al., Mars' Atmosphere: Comparison of Entry Profiles with Numerical Models, 8th International Planetary Probe Workshop poster session, Portsmouth, VA on June 6-10, (2011). **[14]** J. T. Schofield et al., The Mars Pathfinder Atmospheric Structure Investigation/Meteorology Experiment (ASI/MET), Science, 278, pp. 1752-1758, (1997). **[15]** R. T. Clancy & B. J. Sandor, CO_2 ice clouds in the upper atmosphere of Mars, Geophys. Res. Letters, Vol. 25, No. 4, pp. 489-492, (1998). **[16]** D. W. Way et al., Assessment of Mars Science Laboratory Entry, Descent, and Landing Simulation, AAS 13-420, (2013). **[17]** B. R. Cobleigh et al., Flush Airdata Sensing (FADS) System Calibration Procedures and Results for Blunt Forebodies, NASA Technical Report TP-1999-209012, (1999). **[18]** Y. Mignot et al., An insight into EXOMARS EDM HS development, ESA TPS Workshop 7th edition, ESA ESTECT, Noordwijk, The Netherlands on 8-10 April, (2013). **[19]** L. F. Huber, Atmospheric Structure Experiment (ASE) Data Archive (PHX-M-ASE-2-EDL-V1.0), Planetary Data System (PDS) `http://atmos.nmsu.edu/PDS/data/phxase_0001/` on August 2013, (2008). **[20]** P. N. Desai et al., Entry, Descent, and Landing Performance of the Mars Phoenix Lander, J. of Spacecraft and Rockets, Vol. 48, No. 5, (2011). **[21]** B. Van Hove & Ö. Karatekin, Mars Atmosphere Reconstruction using a Flush Air Data System on the ExoMars Entry, Descent and Landing Demonstratore Module, 10th International Planetary Probe Workhop, San Jose State University, CA on 17-21 June, (2013). **[22]** K. T. Edquist, et al., Aerodynamics for Mars Phoenix Entry Capsule, J. of Spacecraft and Rockets, Vol. 48, No. 5, pp. 713–726, (2011). **[23]** J. B. Scoggins, Development of MUTATION++: Multicomponent Thermodynamics And Transport properties for IONized gases library in C++, Rev. of the VKI Doctoral Res., 2012-2013. **[24]** L. V. Lorenzoni, ExoMars 2016 Entry Descent and Landing Demonstrator Module EDL overview, 10th International Planetary Probe Workshop, San Jose State University, CA on 17-21 June, (2013). **[25]** W. B. Banerdt et al., InSight: A discovery mission to explore the interior of Mars, 44th Lunar and Planetary Science Conference, The Woodlands, TX on March 18-22, (2013). **[26]** F. Forget et al., Modeling the martian atmosphere with the LMD global climate model, 3rd International Workshop on the Mars Atmosphere: Modeling and Observations, Williamsburg, VA on 10-13 Nov, (2008). **[27]** M. E. Ockert-Bell et al., Absorption and scattering properties of the Martian dust in the solar wavelengths, J. of Geophys. Res.. Vol. 102, Issue E4, pp. 9039-9050, (1997). **[28]** Communicated by François Forget, 31 May 2013 **[29]** I. A. Johnston, Simulation of Flow Around Hypersonic Blunt Nosed Vehicles for the Calibration of Air Data Systems, PhD thesis, University of Queensland, Dept. of Mechanical Engineering, (1999).